Robust oscillations in multi-cyclic models of biochemical clocks

Clara del Junco and Suriyanarayanan Vaikuntanathan*

Department of Chemistry and The James Franck Institute, University of Chicago, Chicago, IL, 60637

Understanding the physical basis for robust biochemical oscillations in the presence of fluctuations, as observed for instance in circadian oscillators, has emerged as an important problem. In a previous paper (arXiv:1808.04914), we explored this question using the non-equilibrium statistical mechanics of single-ring Markov state models of biochemical networks that support oscillations. Our finding was that they can exploit high affinity to maintain a robust period and coherence in the presence of fluctuations in rates. Here, we extend our work to Markov state models consisting of a large cycle decorated with multiple small cycles. These additional cycles are intended to represent alternate pathways that the oscillator may take as it fluctuates about its average path. Combining a mapping to single-cycle networks based on first passage time distributions with previously developed theory, we are able to make analytical predictions for the period and coherence of oscillations in these networks. One implication of our predictions is that for these networks a high energy budget can make different network topologies and arrangements of rates degenerate as far as the period and coherence of oscillations is concerned. Excellent agreement between analytical and numerical results confirms that this is the case. Our results suggest that biochemical oscillators can be more robust to fluctuations in the path of the oscillator when they have a high energy budget.

I. INTRODUCTION

Many organisms use internal biochemical clocks to synchronize their metabolism to day-night cycles. An internal record of time has been shown to confer fitness to organisms as it allows them to anticipate periodic environmental changes [1]. From a theoretical standpoint, understanding the non-equilibrium statistical mechanical requirements for maintaining robust oscillations in these molecular clocks has emerged as an important question. In particular, the connection between energy dissipation and the coherence of oscillations in a stochastic environment has been noted by many theoretical studies [2–8]. Some of this work proposes thermodynamic bounds which set a lower limit on the extent of stochastic fluctuations in these systems as a function of the energy dissipation budge [2, 4, 6]. However, the structure of even simple models of biochemical oscillators constrains them to operate far from these bounds [8] - i.e., fluctuations are much larger than the minimum for the amount of energy that the oscillator is using. In particular, fluctuations are minimized only in the case of a symmetric oscillator, that is, when all of the clockwise rates k_i^+ in the model in Fig. 1a are equal to one another and related to the counterclockwise rates k_i^- by $k^+ = \exp(\mathcal{A}/N)k^-$ where $\mathcal{A}$ is the affinity, the non-equilibrium driving force that drives the system out of equilibrium which is typically provided by ATP hydrolysis, and N is the size of the cycle.

Recently, we considered how a single-cycle Markov model of an oscillator such as that pictured in Fig. 1a operates when the rates are not symmetric, but rather chosen from a probability and subject to fluctuations, as is reasonably expected in any chemical reaction network operating in a noisy biological environment [9]. By deriving an analytical expression for the period and coherence

of oscillations that reveals their detailed dependence on all of the rates in the network, we showed that in addition to suppressing fluctuations due to the inherent stochasticity of the Poisson hopping events on the ring and the possibility of reverse hops, a high chemical affinity, defined as

$$\mathcal{A} = \sum_{cycle} k_i^+/k_i^-, \tag{1}$$

allows the period of the oscillator to remain more tightly distributed when the rates in the model fluctuate. In this paper, we build on our previous work to further explore this role of energy dissipation. Specifically, we extend our work to networks with multiple cycles and show that the period of the oscillator is more robust at high affinity when the topology of the network fluctuates as well as the rates.

The paper is organized as follows: in Section II we briefly review our analytical theory from Ref. 9. This theory depends on the single-cycle topology of the network, so to apply it to multi-cycle networks such at the one illustrated in Fig. 1b, in Section III we show how to coarse-grain small cycles on to single links, yielding an effective single-cycle network whose period and coherence are meant to approximate those of the full multi-cyclic network. In Section IV we compare these observables calculated numerically in multi-cycle networks to the corresponding coarse-grained networks and analytical approximations, and show that at high affinity our analytical approximation, which takes as input only a small subset of the parameters required to specify the multi-cycle network, accurately reproduces the period and coherence in these networks. We demonstrate the ability of our theory to predict timescales when the rates and topology in the network are randomly generated. Finally, in Section V, we discuss the implications of our results for biochemical oscillators and show one example of how the multi-cycle networks studied here can be used to achieve input com-

---

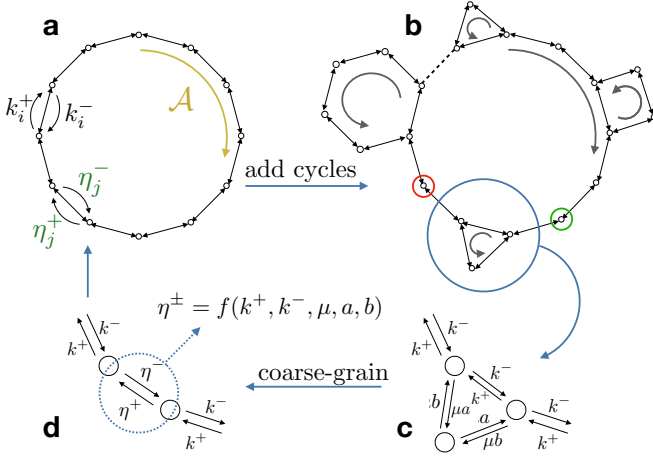* Corresponding Author: svaikunt@uchicago.edu

FIG. 1. A schematic of the networks studied in this article. (a) In previous work [9], we developed an analytical theory for the period of oscillations T and the number of coherent oscillations $\mathcal{R}$, defined in Eq. 2, in oscillators that can be represented by a single cycle of states where the clockwise (CW) hopping rates (k_i^+) are much larger than the counterclockwise (CCW) hopping rates (k_i^-). This asymmetry is quantified by the affinity $\mathcal{A}$, defined in Eq. 1. (b) In this work, we extend our results to networks where the main cycle is decorated with many small cycles. (c) We design these 'decorations' so that the rates going in to them are modulated by a small parameter μ which governs the probability that the system will enter the small cycle. (d) To apply our theory to these multi-cycle networks, we map the muti-cyclic network on to a unicyclic network by matching moments of the first passage time distribution for a random walk beginning CCW from the decoration (green circle) and ending CW from it (red circle) on to a line of states with two unknown hopping rate. This procedure gives a set of effective hopping rates $\eta_i^\pm$. When each of the decorations in the network is coarse-grained in this manner, we obtain a single-cycle network as in (a) whose period T and coherence $\mathcal{R}$ should approximate those of the full, multicycle network.

pensation, which is the ability to maintain a constant period when the affinity changes.

II. ANALYTICAL THEORY FOR TIMESCALES IN SINGLE-CYCLE OSCILLATOR MODELS

In Ref. 9, we derived analytical expressions for the period and coherence of oscillations in a network consisting of a single cycle of states, such as the one depicted in Fig. 1a. In this section, we briefly review that result. Further details are available in Ref. 9. The network is driven out of equilibrium by an affinity, $\mathcal{A}$, defined in Eq. 1 - a finite affinity is necessary to have oscillations. The quantities of interest are two time scales: the average period of oscillations T and the number of coherent oscillations, $\mathcal{R}$, defined as

$$T = 2\pi/|\operatorname{Im}[\phi]| \qquad \mathcal{R} = -|\operatorname{Im}[\phi]|/\operatorname{Re}[\phi] \qquad (2)$$

where ϕ is the eigenvalue of the transition rate matrix of the network that yields the largest value of $\mathcal{R}$ [10]. An exact expression for ϕ in a cycle of N states in the special symmetric case where $k_i^+ = k^+$ and $k_i^- = k^-$ for all i is given by:

$$\phi^{(0)} = -(k^- + k^+) + k^- e^{-2\pi i/N} + k^+ e^{2\pi i/N}. \qquad (3)$$

We then considered networks where at least one of the CW rates is equal to k^+ and at least one of the CCW rates is equal to k^-. The remaining $m \leq N - 1$ rates, denoted $h_j^\pm$, can be selected randomly from a distribution ranging over at least an order of magnitude above or below these "uniform" rates. The main result of Ref. 9 was an expression for ϕ in this setup, in the limit of high affinity where terms of order $k^-/k^+ = \exp(-\mathcal{A}/N)$ can be neglected compared to terms of order 1. The result is summarized in the following expressions:

$$\phi = \phi^{(0)} + C\gamma \qquad (4)$$

$$\phi^{(0)} = -(k^- + k^+) + k^- \exp(-2\pi i/N) + k^+ \exp(2\pi i/N) \qquad (5)$$

$$\gamma = \frac{1}{m-N}\left(\sum_{j=1}^{m} \log\big(\zeta_j(\gamma, k^\pm, h_j^\pm, N)\big)\right) + \frac{1}{2(m-N)^2}\left(\sum_{j=1}^{m} \log\big(\zeta_j(\gamma, k^\pm, h_j^\pm, N)\big)\right)^2 \qquad (6)$$

$$(7)$$

with expressions for $\zeta_j(\gamma, k^\pm, h_j^\pm, N))$ and C given in Appendix A. The essential feature of these equations is that Eq. 6 depends independently on each rate $h_j^\pm$ and does not contain any information about the relative positions of the rates in the network. As a result, in the limit of moderately high affinity, fluctuations in the rates decouple from each other and only contribute additively to

the timescales, and we find that $\mathcal{R}$ and T are insensitive to the arrangement of the rates in the network. From a biological perspective, this means that the farther an oscillator operates from equilibrium, the more robust it will be to fluctuations in the rates.

We note that Eq. 6 is a self-consistent equation for γ. The theoretical predictions in the following section are

obtained numerically by searching for solutions to Eq. 6 near to a linear approximation of Eq. 6.

FIG. 2. Effective rates resulting from the coarse-graining procedure as a function of μ, which controls the probability of entering the triangle. We consider the cases where $b = k^+$ and $a = k^-$ ("trans", a-b) and where $b = k^-$ and $a = k^+$ ("cis", c-f). a-d: relative values of the effective rates $\eta^\pm/k^\pm$ compared to the $\mu = 0$ values. The rates change much more dramatically in the cis case, because an extra, likely path for hopping CCW through the decoration is added. e-f: For the cis case, the absolute value of the effective rates and comparison with the high-affinity expressions given in table I (black dashed lines).

III. MAPPING MULTI-CYCLE TO SINGLE-CYCLE OSCILLATORS VIA FIRST PASSAGE TIME DISTRIBUTIONS

The derivation of Eqs. 4 - 6 used a transfer matrix technique which depended on the single-ring topology of the network. Rather than trying to extend this approach to networks with decorations of the kind we wish to consider here, depicted in Fig. 1a, we took a different approach and chose instead to map multi-cycle networks on to single-cycle networks so that Eqs. 4-6 can then be directly applied to the mapped network. Because we want a mapping that preserves time scales, our approach is to build a single-cycle network with rates such that the mean and variance of the first passage time from a site upstream (in the sense of the probability current) of a decoration to a site downstream of a cycle is preserved (denoted by the green and red circles in Fig. 1b). For each decoration, we replace the rates along the edge shared by the large and small cycles with an effective CW rate η^+ and an effective CCW rate η^-.

In order to do this, we first calculate the first passage time (FPT) distribution across the decoration in the full network in Laplace space [11, 12] (details in Appendix B). Though the Laplace-transformed FPT distribution $\tilde{F}(s)$ may not be easy to invert to obtain the real-time FPT distribution $F(t)$, $\tilde{F}(s)$ is a moment-generating function for $F(t)$, with the nth moment $\langle \tau^n \rangle$ given by:

$$(-1)^n \left(\frac{\partial^n \hat{F}}{\partial s^n} \right)_{s=0} = \langle \tau^n \rangle. \tag{8}$$

For the decoration in Fig. 1c, $\tilde{F}(s)$ is a function of $\mu, a, b, k^+,$ and k^-. For the line of states in Fig. 1d, $\tilde{F}(s)$ is a function of $k^+, k^-,$ and two unknown rates η^+, η^-. By setting the mean and variance of these two FPT distributions equal to one another, we obtain analytical expressions for η^+, η^- in terms $\mu, a, b, k^+,$ and k^-. These expressions are algebraically complicated, so we do not reproduce them here; for the smallest motif considered - a triangle as depicted in Fig. 1c - the full effective rates are given as an example in Appendix C. By calculating effective rates for all of the decorations in a network, we can construct a single-cycle network that we expect to have a similar period T (captured by the first moment of the FPT distribution) and coherence $\mathcal{R}$ (captured by the second moment of the FPT distribution) as the decorated network.

We note that this procedure does not always produce reasonable coarse-grained rates. The effective rates diverge at a value of μ that decreases as the size of the decoration increases (Table I). As the size of the decoration becomes larger, it will be able to support coherent 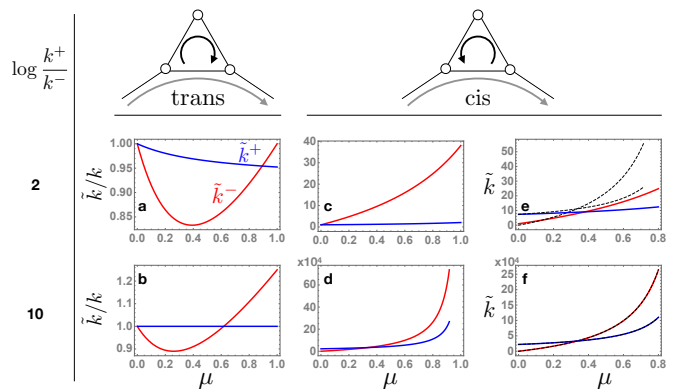oscillations of its own, leading to a system with multiple interacting periods of oscillation; in that case, one cycle is no longer dominant in terms of the dynamics of the system and we do not expect to be able to simply coarse-grain out these competing cycles. We therefore restrict our study to small cycles with 6 sides or fewer where positive effective rates are possible for values of μ of at least $\mu = 0.05$. The effective rates can also become negative if the rates in the main cycle ($k^{+/-}$) and the decoration (a/b) are very (orders of magnitude) different. In the remainder of the paper, we focus on cases where $a = k^-$ and $b = k^+$, which we call "cis" because the rates in the main cycle and decoration favor current in the same direction through their shared edge, or where $a = k^+$ and $b = k^-$, which we call "trans" because the rates in the main cycle and decoration favor current in opposite direction through their shared edge. The relative magnitude of the rates in the decoration compared to the main cycle is tuned by changing μ. The cis configuration favors cycling in the small decoration compared to the trans configuration, as shown schematically in Fig. 2. In Table I we show the effective rates in the cis configuration in the limit where $k^-/k^+ \to 0$ (for the trans configuration this limit simple gives $\eta^+ = k^+$ and $\eta^- = 0$). In Fig. 2 we show $\eta^\pm$ as a function of μ for both configurations. In the cis configuration, η^- quickly becomes larger than η^+ as μ is increased, creating a bottleneck in the network as the system become trapped in the decoration.

Shape	Exclusive Vertices	η^+	η^-
triangle	1	$k^+/(1-\mu)$	$3k^+\mu/(1-\mu)$
square	2	$k^+/(1-3\mu)$	$6k^+\mu/(1-3\mu)$
pentagon	3	$k^+/(1-6\mu)$	$10k^+\mu/(1-6\mu)$
hexagon	4	$k^+/(1-10\mu)$	$15k^+\mu/(1-10\mu)$
general	x	$\frac{2k^+}{2-x(x+1)\mu}$	$\frac{k^+(x+1)(1+x/2)}{2-x(x+1)\mu}$

TABLE I. Effective rates across decorations with increasing number of sides, in the limit of $k^-/k^+ \to 0$. We deduce by inspection that the effective rates for a decoration with x vertices that do not belong to the large cycle are: $\eta^+ = k^+/(1-\alpha\mu)$, $\eta^- = (x+1+\alpha)k^+/(1-\alpha\mu)$ where $\alpha = \sum_{i=1}^{x} i = x(x+1)/2$, as shown in the last row.

IV. PREDICTING TIMESCALES IN MULTICYCLIC NETWORKS

We can now compare T and $\mathcal{R}$ for our coarse-grained networks to the full networks. The *cis* configuration leads to more dramatic changes in the effective rates than the trans configuration (Fig. 2), and we found that as a result $\mathcal{R}$ and T change by only a small fraction as μ in turned on in networks with *trans*-configured decorations. For the results in this section we therefore focus on decorations with *cis* rates. We calculate T and $\mathcal{R}$ in three ways: first, by numerically diagonalizing the transition rate matrix of a network with explicit decorations ($\mathcal{R}/T_{exact}$); second, by numerically diagonalizing the transition rate matrix of the corresponding coarse-grained network ($\mathcal{R}/T_{CG}$), and third, using the theoretical expressions in Eqs. 4 - 6 with the rates in the coarse-grained network as input ($\mathcal{R}/T_{th}$).

In the following sections we test the ability of our coarse-graining scheme combined with our analytical theory to predict T and $\mathcal{R}$ in networks with increasing amounts of randomness. Since our theory does not contain information about the locations of the effective rates in the network, if we are able to predict these observables it means that they are insensitive to the locations of decorations on the network and will be robust to any changes in the locations of the decorations.

A. Networks with symmetrically distributed decorations

First we test the accuracy of the coarse-grained and theoretical approximations for a fixed network topology. In Fig. 3 we show results for networks with a large cycle of size $N = 100$ with a single triangle decoration as a function of μ, and with m evenly spaced triangle decorations as a function of m. When $m = 1$, $T/\mathcal{R}_{CG}$ approaches $T/\mathcal{R}_{exact}$ as the affinity increases, with perfect agreement in the limit of very high affinity ($k^-/k^+ = \exp(-10) \approx 0$). Note that in this limit the effective reverse hopping rates along edges representing coarse-grained decorations are not suppressed; rather
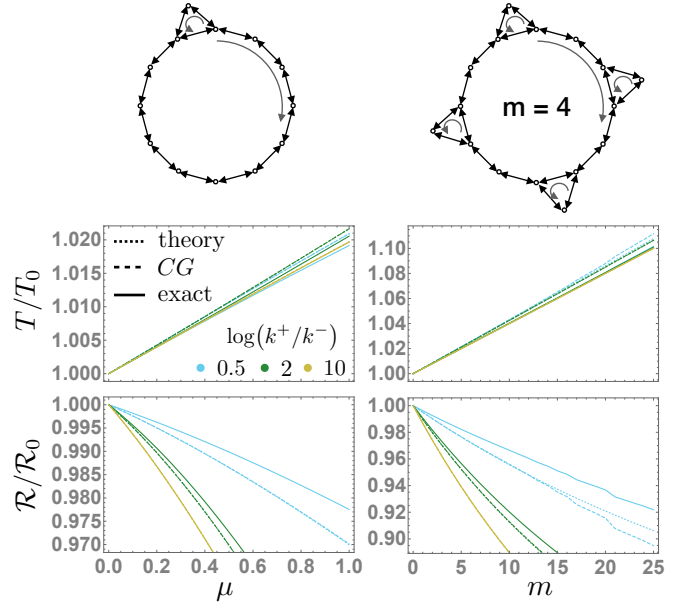

FIG. 3. Period T and number of coherent oscillations $\mathcal{R}$ in networks with $N = 100$ states in the main cycle and triangle decorations with the cis configuration of rates ($a = k^-$, $b = k^+$). We set $k^- = 1$ and set $k^+ = \exp(\mathcal{A}_0/N)$. $\mathcal{A}_0$, R_0 and T_0 are the respective values in a network with no decorations. "Exact" results are calculated from numerical diagonalization of the full network. "CG" results are calculated from numerical diagonalization of a single cycle with $N = 100$ states with effective rates through the links where decorations are located in the full network. "Theory" results are calculated from the theoretical expression in Eqs. 4 - A9 with the rates $\{h_j\}$ given by the effective rates. On the left we show results for networks with one triangle decoration, as a function of μ, which governs the probability of entering the decoration (see Fig. 1). On the right, we show results for networks with $\mu = 0.2$ fixed and with m triangle decorations separated by $\lfloor N/m \rfloor$ edges. This value jumps when $N\%m = 0$, resulting in the observed discontinuous changes at these values when $\mathcal{A}_0/N = 0.5$.

they are enhanced (Fig. 2) and $\eta^-/\eta^+ > 1$ (Fig. 2f), so that even in the limit $k^-/k^+ \to 0$ it is non-trivial to predict the period. The agreement between $T/\mathcal{R}_{th}$ is also excellent. The net effect is convergence between exact values and theoretical predictions for T and $\mathcal{R}$ with increasing affinity.

The distance between decorations is given by $\lfloor N/m \rfloor$. At low affinity, this results in discontinuous jumps in the values of $T/\mathcal{R}_{exact}$ and $T/\mathcal{R}_{CG}$ (yellow lines in right column of Fig. 3) at values of m where the N is an integer multiple of m, because the distance between the decorations is important. At high affinity the distance no longer matters, as predicted by our theory, and the CG and exact lines become smooth and ultimately match the theory prediction.
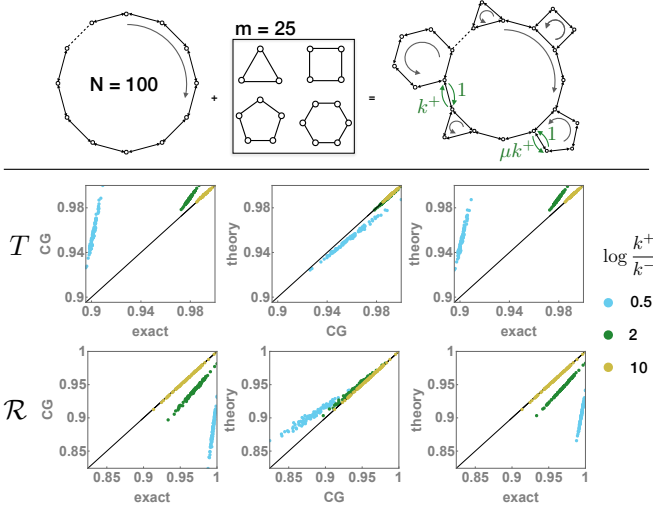
FIG. 4. Period T and number of coherent oscillations $\mathcal{R}$ in networks with $N = 100$ states in the main cycle and $m = 25$ decorations whose shape and location are randomly generated, with the constraint that no vertex is connected to more than three neighbors, i.e. the decorations are separated by at least one edge. The rates are chosen as in Fig. 3, except that we chose $\mu = 0.05$ since the effective rates for larger decorations diverge at decreasing values of μ (see Table I). Each point in the scatter plots represents a specific realization of quenched disorder of shapes and locations. As $\mathcal{A}_0/N = \log\left(k^+/k^-\right)$ increases, the exact, coarse-grained and theory values converge. All values are normalized by the largest value in the data on each scatter plot so that data for different affinities can be shown on the same plot.

B. Networks with randomly distributed decorations

The success of our theory in predicting time scales in Fig. 3 suggests that networks with many different arrangements of the same set of decorations, or of similar sets drawn from a common distribution, will have the same values of T and $\mathcal{R}$. We now introduce disorder by fixing the number of decorations $m = 25$ and the value of $\mu = 0.05$ and selecting the shapes and locations of decorations in the network randomly. Because our coarse-graining scheme takes in to account the edges CW and CCW from the decoration as shown in Fig. 1b, we do not expect it to work well when two decorations are connected to the same vertex, and we constrain the random locations so that this does not happen (i.e. decorations are separated by at least one edge). The decorations may have between 3 and 6 sides. Scatter plots in which each point represents one realization of the quenched shape and location disorder are shown in Fig. 4. The results show that in these disordered networks, the exact, CG, and theory results converge at high affinity, confirming that the arrangement of decorations is unimportant at high affinity.
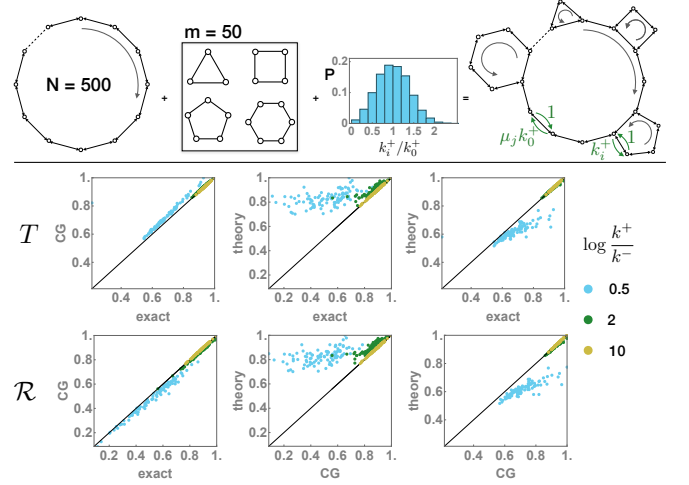
FIG. 5. Period T and number of coherent oscillations $\mathcal{R}$ in networks with $N = 500$ states in the main cycle and $m = 50$ decorations. Here, disorder in the rates of the main cycle as well as disorder in the topology of the network are considered. The shapes and locations of the decorations are randomly generated, with the constraint that the decorations are separated by at least two edges. Then, rates along edges in the main cycle which are not connected to a vertex which is part of a decoration are randomly chosen from a Gaussian distribution with mean k_0^+ and standard deviation $0.4k_0^+$ and a lower cutoff at $0.1k_0^+$, and the locations of the decorations were randomly selected with the constraint that no node is connected to more than 3 neighbors (i.e. no decorations right next to one another). We set $a = k^- = 1$ and $b = k_0^+ = \exp(\mathcal{A}_0/N)$. We introduced disorder in the probability of entering the decorations by choosing μ randomly from a uniform distribution $[0, 0.95\mu_{max}]$, where μ_{max} is the value of μ at which the effective rates in Table I diverge, which depends on the shape of the decoration. Each point in the scatter plots represents a specific realization of quenched disorder of shapes, locations, and rates. As $\mathcal{A}_0/N = \log\left(k^+/k^-\right)_0$ increases, the exact, coarse-grained and theory values converge. All values are normalized by the largest value in the data on each scatter plot so that data for different affinities can be shown on the same plot.

C. Combining rate disorder and topological disorder

Finally, we test how our theory performs when disorder in the rates, explored in Ref. 9, is combined with random network topology (Fig. 5). We now generate networks with large cycles of size $N = 500$ and $m = 50$ decorations with random shapes and random locations. The locations are again constrained so that no two decorations are connected to the same vertex. The rates in the large cycle that are not part of the coarse-grained motif (i.e., are not connected to a vertex which is part of a decoration) are then chosen randomly, as are the values of μ. We set the rates in the motifs to the cis configuration. Once again, the agreement between both levels of approximation and exact results for T and $\mathcal{R}$ is excel-
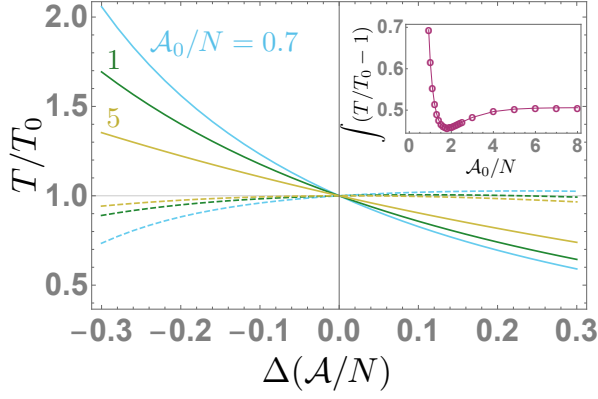
FIG. 6. Compensating for changes in period by tuning the parameter μ as a function of $\Delta\mathcal{A}$ in a network with a large cycle of $N = 100$ states with $m = 20$ triangle decorations symmetrically distributed on the network, with the cis configuration $(a = k^{-} = 1, b = k^{+} = \exp(\mathcal{A}/N) = \exp((\mathcal{A}_0 + \Delta\mathcal{A})/N))$. T_0 is the period at $\mathcal{A}_0/N$ and $\mu_0 = 0.5$. Dashed lines are the period as the affinity is changed with $\mu = \mu_0$; solid lines are the period when μ is changed as a function of the affinity: $\mu = \mu_0 + \Delta\mu$ with $\Delta\mu = \kappa_{comp}\Delta\mathcal{A}$, as described in the text. This linear compensation mechanism is effective over a wide range of affinities $\mathcal{A}_0$, compensating for changes in period of $\sim 50\%$. Compensation occurs because by increasing (decreasing) μ the system is encouraged to spend more (less) time in the triangle decorations as the affinity is increased (decreased). Inset: The integrated deviation from perfect compensation ($T/T_0 = 1$) over the range $\Delta\mathcal{A} \in [-0.3, 0.3]$ as a function of the affinity in the unperturbed network. The mechanism is most effective when $\mathcal{A}_0/N \approx 2$ or greater.

lent in the limit of high affinity ($k^{+}/k^{-} = \exp(10)$), with very good agreement already at moderate values of the affinity ($k^{+}/k^{-} = \exp(2)$).

V. DISCUSSION

The results of Fig. 5 show that the time scales of an oscillator with multiple cycles and randomly distributed rates does not depend on the arrangement of these rates and cycles. As a result, these observables can be accurately predicted from our theory with information about the probability distributions of the rates and decorations, and notably without information about the spatial arrangement of the specific network. This extends the conclusions of Ref. [9] to the case of network topology. The motivation for studying multiple cycles is that the small cycles can represent deviations from or noise in the oscillator's average limit cycle [8, 13]. The quenched disorder in Figs. 4 and 5 are meant to represent different realizations of the pathways sampled by the oscillator over time. In this context, our results show how an oscillator whose sampled paths and rates are fluctuating over time can use a high chemical affinity to maintain a predictable and robust period.

We now briefly turn our attention from local, rapidly

decaying fluctuations to global, long-lived fluctuations; e.g. a change in the affinity due to a shift in the overall ATP to ADP ratio in a cell, caused for instance by a change in light levels or a change in temperature. Biochemical oscillators often have the ability to maintain a constant period in the presence of a certain range of these changes, a feature known as input compensation [14–16]. For a given network topology and arrangement of relative rate magnitudes, changing the affinity effectively multiplies all of the rates by a constant since $k^{+}/k^{-} \propto \exp(\mathcal{A}/N) = \exp(\mathcal{A}_0/N)\exp(\Delta\mathcal{A}/N)$. Any change in the affinity therefore results in a change in the period. However, if the rates or the decorations in the network are allowed to vary in a manner that is coupled to the change in affinity, the oscillator may be able to absorb changes in the affinity. Specifically, if the current increases on the network in response to an increase in the affinity, the system can increase the path length by increasing the probability of entering and remaining in small cycles. This mechanism for compensation is a stochastic version of one that has previously been explored in deterministic limit cycles by several authors [15, 17]: if an input changes the angular velocity of the limit cycle, the radius of the limit cycle must also change in response to the input in order to maintain a constant period. Similarly, in our multi-cycle networks, the length of the path that the system takes to complete one full oscillation is tuned by the arrangement and rates of decorations in the network.

We illustrate an example of this in Fig. 6. We choose the rates in the network as in Fig. 3: $a = k^{-} = 1$, $b = k^{+} = \exp(\mathcal{A}/N)$. First we hold μ fixed and vary the affinity so that the rates become $b = k^{+} = \exp(\mathcal{A}_0 + \Delta\mathcal{A}/N)$, and show that the period changes significantly with small changes in the affinity (solid lines in Fig. 6) - for instance, changing the affinity from $\mathcal{A}_0/N = 5$ to $\mathcal{A}/N = 5.3$ reduces the period by 25%. Then, we allow the value of μ to be appropriately coupled to the affinity and show that these changes in the period can be compensated for, reducing the change to less than 5%. The parameter μ controls the probability of accessing the smaller secondary cycles. Hence, the parameter μ effectively controls the size of sampled orbits in our networks.

In order to choose how μ should be depend on the affinity, we consider the Taylor expansion of the period as a function of $\mathcal{A}$ and μ:

$$T(\mathcal{A}, \mu) = T(\mathcal{A}_0, \mu_0) \tag{9}$$
$$+ \left(\frac{\partial T(\mathcal{A}_0, \mu_0)}{\partial \mu}\right)\Delta\mu + \left(\frac{\partial T(\mathcal{A}_0, \mu_0)}{\partial \mathcal{A}}\right)\Delta\mathcal{A}$$
$$+ \mathcal{O}((\Delta\mu)^2, (\Delta\mathcal{A})^2, \Delta\mu\Delta\mathcal{A}) + \cdots$$

Perfect compensation then requires $T(\mathcal{A}, \mu) = T(\mathcal{A}_0, \mu_0)$ or

$$0 = \left(\frac{\partial T(\mathcal{A}_0, \mu_0)}{\partial \mu}\right)\Delta\mu + \left(\frac{\partial T(\mathcal{A}_0, \mu_0)}{\partial \mathcal{A}}\right)\Delta\mathcal{A} + \cdots \tag{10}$$

In general this leads to a very complicated function of

$\Delta\mu(\Delta\mathcal{A})$ with as many parameters as the Taylor expansion has terms. However, in Fig. 6 we find numerically that over wide ranges of change in the period, it is in fact a linear function of $\Delta\mathcal{A}$ and $\Delta\mu$, so that we can achieve compensation just by setting

$$\Delta\mu = -\left[\left(\frac{\partial T(\mathcal{A}_0,\mu_0)}{\partial\mathcal{A}}\right)\bigg/\left(\frac{\partial T(\mathcal{A}_0,\mu_0)}{\partial\mu}\right)\right]\Delta\mathcal{A} \quad (11)$$

$$\equiv \kappa_{comp}\Delta\mathcal{A}. \quad (12)$$

In the inset in Fig. 6, we see that this 'linear compensation' mechanism works best above a minimum value of the affinity around $\mathcal{A}_0/N = 1$, indicating that a high chemical affinity can support simple mechanisms for compensation. Indeed, using a linear approximation of our theory in Eqs. 4 - 6, we find that as long as the effective rates in the coarse-grained link are proportional to k^+ (as they are in our case; see Table I), all second-order and higher terms in Eq. 10 vanish at high affinity and for large main cycle size N. High affinity therefore makes it easy to design (or evolve) a network of this kind with compensation, since only one parameter needs to be set, which is easily computed from the unperturbed $(\mu_0, \mathcal{A}_0)$ network.

Here we have illustrated compensation using μ for simplicity since it is a continuous variable. However, the number of decorations or the size of the decorations could also be used to adjust the period, since these all affect the path length of an oscillation, or alternately, the amount the time the system spends effectuating futile cycles in decorations. This, and related additional mechanisms for compensation will be explored in future work.

VI. CONCLUSION

In this paper we presented an analytical theory for computing the period of oscillations in Markov models consisting of one large cycle of size N decorated with a fraction of smaller secondary cycles that are driven out of equilibrium by an affinity $\mathcal{A}$ (Fig. 1). First, we mapped the decorations on to single links that retain the mean and variance of the first passage time across the decoration. Performing this procedure for all of the decorations

in the network yields a single-cycle network for which we have previously derived an analytical expression for the period and coherence of oscillations. Importantly, the analytical expression takes as input the rates along each edge in the network, but does not know about their relative placement. Numerical calculations of the period at high affinity agree well with this analytical prediction (Figs. 3 - 5). Our main result is that the ability of our theory to accurately predict the period and coherence implies that high energy dissipation makes these observables insensitive tomany parameters; specifically, the arrangement of the cycles and rates in the network. As a result, oscillators represented by the models studied here can have time scales that are robust to fluctuations in rates and topology that decay over time scales comparable to the period. Finally, we showed how multi-cycle network topologies can also be exploited to achieve compensation to long-lived, global rate fluctuations due to changes in affinity, by tuning the amount of time that the system spends in the small cycles.

[1] M. A. Woelfle, Y. Ouyang, K. Phanvijhitsiri, and C. H. Johnson, Current Biology **14**, 1481 (2004).
[2] A. C. Barato and U. Seifert, Physical Review Letters **114**, 158101 (2015).
[3] Y. Cao, H. Wang, Q. Ouyang, and Y. Tu, Nature Physics **11**, 772 (2015).
[4] A. C. Barato and U. Seifert, Physical Review E **95**, 062409 (2017).
[5] C. Fei, Y. Cao, Q. Ouyang, and Y. Tu, Nature Communications **9**, 1434 (2018).
[6] H. Wierenga, P. R. Ten Wolde, and N. B. Becker, Physical Review E **97**, 042404 (2018).
[7] B. Nguyen, U. Seifert, and A. C. Barato, The Journal of Chemical Physics **149**, 045101 (2018).
[8] R. Marsland, W. Cui, and J. M. Horowitz, Journal of The Royal Society Interface **16**, 20190098 (2019).
[9] C. del Junco and S. Vaikuntanathan, (2018), arXiv:1808.04914.
[10] In refs. 9 and 4, ϕ was defined as the eigenvalue with the least negative real part. However, in the multicyclic networks we address later in this paper, that definition can

lead to selecting an eigenvalue which corresponds to cycling around a decoration rather than global oscillations.

[11] A. Murugan, D. A. Huse, and S. Leibler, Proceedings of the National Academy of Sciences of the United States of America **109**, 12034 (2012).

[12] S. Budnar, K. B. Husain, G. A. Gomez, M. Naghibosadat, A. Varma, S. Verma, N. A. Hamilton, R. G. Morris, and A. S. Yap, Developmental Cell **49**, 894 (2019).

[13] W. Pittayakanchit, Z. Lu, J. Chew, M. J. Rust, and A. Murugan, eLife **7** (2018), 10.7554/eLife.37624.

[14] C. H. Johnson, P. L. Stewart, and M. Egli, Annual review of biophysics **40**, 143 (2011).

[15] P. François, N. Despierre, and E. D. Siggia, PLoS Computational Biology **8**, e1002585 (2012).

[16] J. Paijmans, D. K. Lubensky, and P. R. ten Wolde, Biophysical Journal **113**, 157 (2017).

[17] T. S. Hatakeyama and K. Kaneko, Physical Review Letters **115**, 218101 (2015).

Appendix A: Theory from Ref. 9

Our theory in uses a transfer matrix formulation of the eigenvalue equation for the transition rate matrix of a single-cycle network of size N:

$$\begin{bmatrix} f_1 \\ f_2 \end{bmatrix} = \mathbf{A}\mathbf{B}^{N-1} \begin{bmatrix} f_1 \\ f_2 \end{bmatrix} \tag{A1}$$

where f_i are eigenvector elements, $\mathbf{B}$ is a transfer matrix mapping eigenvector magnitudes about links with 'uniform rates' $k^{\pm}$, and $\mathbf{A}$ is a transfer matrix mapping eigenvector magnitudes about links with 'defect rates' $h^{\pm}$. $\mathbf{A}$ and $\mathbf{B}$ are functions of the eigenvalue ϕ of the transition rate matrix. By Eq. A1, $\mathbf{A}\mathbf{B}^{N-1}$ must have an eigenvalue of one. We postulate $\phi = \phi^{(0)} + C\gamma$ with C given in Eq. A8. Therefore, Eq. A1 is a self-consistent equation for γ which we solve as described in Ref. 9 to obtain Eq. 6. Eq. A1 formula easily to cases where there

is more than one set of defect rates; further details can be found in the Supplementary Material of Ref. 9.

In Ref. 9 we approximated the product of transfer matrices as:

$$\mathbf{A}\mathbf{B}^{N-1} \approx \mathbf{A} \left[\left(\beta_1^{(1)}\right)^{N-1} \mathbf{X}_1^{(0)} + \left(\beta_2^{(1)}\right)^{N-1} \mathbf{X}_2^{(0)} \right] \tag{A2}$$

$$\approx \left(\beta_1^{(1)}\right)^{N-1} \mathbf{A}\mathbf{X}_1^{(0)} \tag{A3}$$

where $\beta_1^{(1)} = \exp(2\pi i/N)(1+\gamma) = \beta_1^{(0)}(1+\gamma)$ and $\beta_2^{(1)} = (k^-/k^+)\exp(2\pi i/N)(1+\gamma) = \beta_2^{(0)}(1+\gamma)$ are first-order perturbed eigenvalues of $\mathbf{B}$, and $\mathbf{X}_i^{(0)} = |i\rangle\langle i|$ is the outer product of the ith unperturbed eigenvectors. In the second line we have assumed high affinity : $k^-/k^+ \ll 1$. The ith left and right eigenvectors of $\mathbf{B}$ are given by:

$$\langle i| = \{-1/\beta_j, 1\}/c_i^2 \qquad |i\rangle = \{\beta_i, 1\}/c_i^2 \tag{A4}$$

where c_i is a normalization constant. Therefore, by using $\mathbf{X}_1^{(0)}$, our theory ignored important terms containing γ. In cases where $k^-/k^+ \ll 1$ and $h^-/h^+ \ll 1$, we find that these terms cancel and our theory works with $\mathbf{X}_1^{(0)}$, explaining the success of our theory in predicting timescales in Ref. 9. However, in the coarse-grained networks studied in this paper we typically find $h^-/h^+ > 1$. We therefore replace

$$\mathbf{X}_1^{(0)} = \frac{1}{c_1^2} \begin{bmatrix} -\beta_1^{(0)}/\beta_2^{(0)} & \beta_1^{(0)} \\ -1/\beta_2^{(0)} & 1 \end{bmatrix} \tag{A5}$$

$$\rightarrow \mathbf{X}_1^{(1)} = \frac{1}{c_1^2} \begin{bmatrix} -\beta_1^{(1)}/\beta_2^{(1)} & \beta_1^{(1)} \\ -1/\beta_2^{(1)} & 1 \end{bmatrix} \tag{A6}$$

in Eq. A3, and proceed with the calculation as described in the Supplementary Material of Ref. 9, to obtain Eqs. 4 - 6, where

$$\zeta_j = \frac{h_j^- k^+ + h_j^+ k^- - k^- k^+ + 2\gamma h_j^+ k^- + \gamma^2 \left(h_j^+ k^- + k^- k^+\right) + (\gamma+1)k^+ e^{\frac{2i\pi}{N}}(-h_j^- - h_j^+ + k^- + k^+) - \left((\gamma+1)k^+ e^{\frac{2i\pi}{N}}\right)^2}{(\gamma+1)h_j^+ \left(k^- - k^+ e^{\frac{4i\pi}{N}}\right)} \tag{A7}$$

$$C = c_1^2 k^- e^{-2\pi i/N} \tag{A8}$$

$$c_1^2 = 1 - (k^+/k^-)e^{4\pi i/N}. \tag{A9}$$

Appendix B: Calculating the first passage time distribution

The method for calculating the first passage time between two states is to sum over all of the paths of all lengths connecting the two states. First we write down

the FPT distribution between two connected states 1 and 2. If the system enters state 1 at time t_0, the probability that it hops to state j at time $t_1 = t_0 + \mu t$ is:

$$Q_{12}(\mu t) = P_{12}(\mu t) \prod_{i \neq 1,2} \left(1 - \int_0^{\mu t} dt P_{1i}(t) \right) \quad \text{(B1)}$$

Where $P_{12}(t) = k_{12} \exp(-k_{12}t)$ is the waiting time distribution for hopping from state 1 to 2. The first term is the probability of hopping at exactly time t_1, while the term in parentheses is the probability that the system has not hopped to any other state in the meantime, because of course it can no longer make the transition $1 \rightarrow 2$ at time t_1 if it's no longer in state 1. The net waiting time distribution out of state 1 is just the sum over connected states: $\sum_j Q_{1j}$.

The probability of observing a particular trajectory with transitions $\{1 \rightarrow 2, 2 \rightarrow 3, \cdots n-1 \rightarrow n\}$ occurring at times $\{t_1, t_2, t_3, \cdots, t_{n-1}\}$ is:

$$Q_{12}(t_1)Q_{23}(t_2 - t_1) \cdots Q_{n-1,n}(t_{n-1} - t_{n-2}). \quad \text{(B2)}$$

Note that state 1 is the first state that the system visits, it is not necessarily a state with a fixed label. In other words, state 1 and state 3 could both be the same state i, if the system jumps back to state i after leaving it. State n is the only state that can be visited only once, since it is an absorbing state.

To obtain the first passage time distribution $F(n, t_{n-1}|1,0)$ we sum over all trajectories that start at state 1 at time t_0 and arrive, for the first time, at state n at time t_{n-1}. We integrate over all possible combinations of transition times $\{t_1, \cdots t_{n-2}\}$ constrained such that t_{n-1} is fixed, and sum over all paths that the system can take:

$$F(n, t_{n-1}|1,0) = \quad \text{(B3)}$$
$$\sum_{paths} \int dt_1 \cdots dt_{n-2} Q_{12}(t_1) \cdots Q_{n-1,n}(t_{n-1} - t_{n-2}).$$

We can turn this convolution in to a product by taking

the Laplace transform:

$$\hat{Q}_{ij} = \int_0^\infty dt e^{-st} P_{ij}(t) \prod_{k \neq i,j} \left(1 - \int_0^t dt' P_{ik}(t') \right) \quad \text{(B4)}$$

so that we have

$$\hat{F}(n, t_{n-1}|1,0) = \sum_{paths} \hat{Q}_{12} \times \hat{Q}_{13} \cdots \hat{Q}_{n-1,n}. \quad \text{(B5)}$$

Since each transition in our Markov model is a Poisson process, we plug in an exponential form for P, giving:

$$\hat{Q}_{ij}(s) = \quad \text{(B6)}$$
$$k_{ij} \int_0^\infty dt e^{-st} e^{-k_{ij}t} \prod_{k \neq i,j} \left(1 - k_{ik} \int_0^t dt' e^{-k_{ik}t'} \right) \quad \text{(B7)}$$
$$= \frac{k_{ij}}{s + \sum_{k \neq i} k_{ik}}. \quad \text{(B8)}$$

To sum over paths we will construct a matrix $\mathbf{K}$ with elements

$$K_{ij} = \begin{cases} \hat{Q}_{ij}(s) & \text{if states i and j are connected} \\ 0 & \text{otherwise} \end{cases} \quad \text{(B9)}$$

K_{1n} then gives us the waiting time distributions for all paths of length 1 from state 1 to n. $[K^2]_{1n}$ gives us paths of length 2, and $[K^m]_{1n}$ gives all paths of length m. Summing,

$$\hat{F}(n, t_{n-1}|1,0) = 1 + K_{1n} + [K^2]_{1n} + \cdots \quad \text{(B10)}$$
$$= \sum_{m=0}^\infty [K^m]_{1n} \quad \text{(B11)}$$
$$= [(\mathbb{1} - \mathbf{K})^{-1}]_{1n}. \quad \text{(B12)}$$

All elements of the matrix are strictly less than 1 since s is always positive, so the Frobenius norm of the matrix $\lim_{m \rightarrow \infty} \mathbf{K}^m < 1$ and the series converges. We can then either invert the Laplace transform to obtain the FPT distribution $F(t)$, or if that's not tractable, we can obtain the moments of the distribution using Eq. 8, which is what we do in this paper.

Appendix C: Effective rates for a triangle decoration

$$d\eta^+ = (k^- + k^+)^2 \left(a^2\mu + k^+(a+b)\right)^2 \tag{C1}$$

$$
\begin{aligned}
d\eta^- = {}& \mu^3 a^3 b k^{+2} \\
& + \mu^2 ab \left[ab(k^- + k^+)^2 + ak^+ \left(-k^{-2} - 2k^-k^+ + k^{+2}\right) + k^{+3}(b + k^- + k^+) \right] \\
& + \mu \left[a^3 k^- (k^- + k^+)^2 - a^2 (k^- + k^+)^2 (k^+(k^- + k^+) - bk^-) \right. \\
& \quad + ak^+ \left(b^2(k^- + k^+)^2 - bk^-k^+(k^- + 2k^+) + k^{+2}(k^- + k^+)^2 \right) \\
& \quad \left. + bk^+ \left(b^2(k^- + k^+)^2 + bk^{+3} + k^{+3}(k^- + k^+) \right) \right] \\
& + k^-k^+(a+b)^2(k^- + k^+)^2
\end{aligned}
\tag{C2}
$$

$$
\begin{aligned}
d = {}& \mu^3 a^3 b k^- \\
& + a\mu^2 \left[a^2(k^- + k^+)^2 + ab \left(k^{-2} + 4k^-k^+ + k^{+2} \right) + bk^+(bk^- - k^+(k^- + k^+)) \right] \\
& + \mu \left[a^3(k^- + k^+)^2 + a^2(k^- + k^+)^2(b + k^- + 2k^+) \right. \\
& \quad \left. - ak^+ \left(k^+(k^- + k^+)^2 - b(2k^- + k^+)(k^- + 2k^+) \right) + bk^{+2}(bk^- - k^+(k^- + k^+)) \right] \\
& + k^+(a+b)^2(k^- + k^+)^2
\end{aligned}
\tag{C3}
$$